Projected increase of Arctic coastal erosion and its sensitivity to warming in the 21st Century

David Nielsen (david.nielsen@uni-hamburg.de)
University of Hamburg https://orcid.org/0000-0003-4201-0373
Patrick Pieper
University of Hamburg
Armineh Barkhordarian
University of Hamburg
Paul Overduin
Alfred Wegener Institute for Polar and Marine Research
Tatiana Ilyina
Max Planck Institute for Meteorology https://orcid.org/0000-0002-3475-4842
Victor Brovkin
Max Plank Institute for Meteorology https://orcid.org/0000-0001-6420-3198
Johanna Baehr
University of Hamburg
Mikhail Dobrynin
University of Hamburg

Article

Keywords: climate change, erosion coastal erosion, permafrost

Posted Date: June 25th, 2021

DOI: https://doi.org/10.21203/rs.3.rs-634673/v1

Version of Record: A version of this preprint was published at Nature Climate Change on February 14th, 2022. See the published version at https://doi.org/10.1038/s41558-022-01281-0.

Projected increase of Arctic coastal erosion and its sensitivity to warming in the 21st Century

David Marcolino Nielsen[1,2,*], Patrick Pieper[1], Armineh Barkhordarian[1], Paul Overduin[3], Tatiana Ilyina[4], Victor Brovkin[1,4], Johanna Baehr[1], and Mikhail Dobrynin [5,1]

[1]Center for Earth System Research and Sustainability (CEN), Universität Hamburg, Hamburg, Germany

[2]International Max Planck Research School on Earth System Modelling, Max Planck Institute for Meteorology, Hamburg, Germany

[3]Alfred Wegener Institute Helmholtz Centre for Polar and Marine Research, Potsdam, Germany

[4]Max Planck Institute for Meteorology, Hamburg, Germany

[5]Deutscher Wetterdienst, Hamburg, Germany

[*]Correspondence to: david.nielsen@uni-hamburg.de

June 16, 2021

Abstract

Arctic coastal erosion damages infrastructure, threatens coastal communities, and releases organic carbon from permafrost. However, the magnitude, timing and sensitivity of coastal erosion increase to global warming remain unknown. Here, we project the Arctic-mean erosion rate to roughly double by 2100 and very likely exceed its historical range of variability by mid-21st century. The sensitivity of erosion to warming also doubles, reaching 0.4-0.5 m year^{-1} °C^{-1} and 2.3-2.8 TgC year^{-1} °C^{-1} by the end of the century under moderate and high-emission scenarios. Our first 21st-century pan-Arctic coastal erosion rate projections should inform policy makers on coastal conservation and socioeconomic planning. Our organic carbon flux projections also lay out the path for future work to investigate the impact of Arctic coastal erosion on the changing Arctic Ocean, on its role as a global carbon sink, and on the permafrost-carbon feedback.

Main

Arctic coast erosion is caused by a combination of thermal and mechanical drivers. Permafrost thaw and ground-ice melt lead to soil decohesion and slumping, while surface ocean waves mechanically abrade the Arctic coast [1]. Sea-ice loss expands the fetch for waves [2, 3], and prolongs the open-water season, increasing the vulnerability of the Arctic coast to erosion [4, 5]. In the past decades, coastal retreat rates have increased throughout the Arctic, often by a factor of two or more [6–10]. The historical acceleration of erosion in the Arctic is linked with the observed decreasing

sea-ice cover [2, 4, 11], increasing air surface [12, 13] and permafrost temperatures [14]. As for the future, Arctic surface air temperature is projected to exceed its natural range of variability within the next decades [15]. Arctic sea ice decline has already exceeded natural variability [15], and summer ice-free conditions are projected by mid-21st century [16]. New regimes of surface waves are also projected in the Arctic Ocean and along the coast [17–19]. Consequently, Arctic coastal erosion rates are expected to increase in the coming decades. However, the extent of this increase is still unknown, as no projections of Arctic coastal erosion rates are available. To fill this gap, we present the first 21st-century projections of coastal erosion at the pan-Arctic scale.

The thawing of permafrost globally releases organic carbon (OC) and increases atmospheric and oceanic greenhouse gas concentrations, feeding back to further warming [20–23]. Arctic coastal erosion alone releases about as much OC as all the Arctic rivers combined [23, 24], fueling about one-fifth of Arctic marine primary production [25]. Despite consistent improvements in the representation of permafrost dynamics [26, 27], the current generation of Earth system models (ESMs) does not account for abrupt permafrost thaw, which may cause projections of OC losses to be largely underestimated [28, 29]. Arctic coastal erosion is one form of abrupt permafrost thaw [22] and a relevant component of the Arctic carbon cycle [23, 30]. Nonetheless, it has not been considered in climate projections so far. The scale mismatch between Arctic coastal erosion and modern ESMs requires the development of holistic models, that account for the key large-scale processes to bridge this gap [30–32].

In this study, we present a novel approach to represent Arctic coastal erosion at the scales of modern ESMs. We develop a semi-empirical Arctic coastal erosion model combining observations from the Arctic Coastal Dynamics (ACD) database [33], climate reanalyses, ESM and ocean surface wave simulations. Our model considers the main thermal and mechanical drivers of erosion as dynamical variables, represented by yearly-accumulated positive temperatures and significant wave heights, and constant ground-ice content from observations. Our approach allows us to make 21st-century projections of coastal erosion at the pan-Arctic scale. We quantify the magnitude, timing and sensitivity of Arctic coastal erosion and its associated OC loss in the context of climate change.

Emergence of Arctic coastal erosion

We project the Arctic-mean coastal erosion rate to increase from 0.9$\pm$0.4 m/year during the historical period (1850-1950) to between 2.0$\pm$0.7 and 2.6$\pm$0.8 m/year by the end of the 21st Century (2081-2100), in the context of anthropogenic climate change, according to the socio-economic pathway (SSP) scenarios SSP2-4.5 and SSP5-8.5, respectively (Fig. 1a). This translates to an increase of the Arctic-mean coastal erosion rate by a factor of about between 2.2 and 2.9 by the end of the century with respect to the historical period. The SSP2-4.5 and SSP5-8.5 scenarios describe medium and high radiative forcings due to greenhouse gas emissions [34], respectively, and include the pathway of the current cumulative CO_2 emissions [35]. In both scenarios, our projections show that the Arctic-mean erosion exceeds its historical range of variability before the end of the century (Fig. 1b).

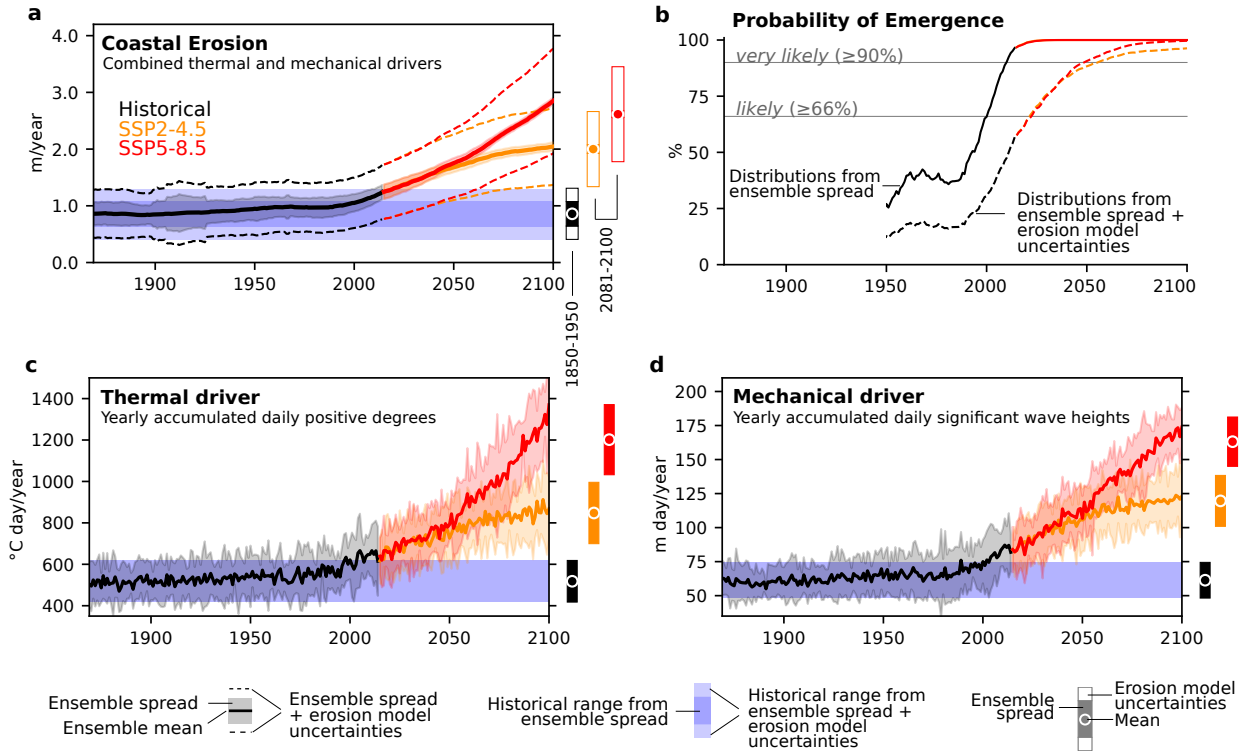

Figure 1: Arctic coastal erosion projections. a) Time evolution of the Arctic-mean coastal erosion rate, expressed as the combined effect of its thermal and mechanical drivers. **b)** Yearly probabilities that the Arctic-mean coastal erosion rate leaves the historical range of variability, calculated from distributions of ensemble spread and erosion model uncertainties (see Methods). In both scenarios, it is very likely (>90% probability) that the Arctic-mean erosion emerges from its historical range by mid 21st century, although the exact time of emergence is sensitive to our erosion model uncertainties. The thermal **(c)** and mechanical **(d)** drivers of erosion, expressed as yearly-accumulated daily positive degrees and significant wave heights, respectively. The erosion time series depict long-term means and therefore show little interannual variability in comparison to its drivers.

We find it likely (≥66% probability) that the Arctic-mean erosion exceeds its historical range by around 2023, and very likely (≥90% probability) by 2049 (Fig. 1b), considering the largest distributions of uncertainties in our projections (i.e. ensemble spread and erosion model uncertainties). The emergence of the Arctic-mean erosion rate would very likely have happened by around 2010,if we take only the ensemble spread to define the historical range. Significant differences in projections between the two scenarios are only noticeable in the second half of the century, after a complete emergence from the historical range. Our erosion time-of-emergence estimates reflect those of its drivers, which take place around mid-21st Century (Fig. 1c,d), in accordance with previous studies [15, 16].

Arctic coastal erosion is typically caused by a combination of thermo-denudation (TD) and thermo-abrasion (TA) [1], which act together to thaw permafrost, melt ground ice, abrade and transport coastal material off shore. We take yearly-accumulated daily positive temperatures and significant wave heights to represent TD and TA: hereafter, the *thermal* and *mechanical* drivers of erosion, respectively. As various landform types compose the Arctic coast, the relative contribution of the thermal and mechanical drivers differs at the local scale. Erosion is predominantly thermally driven at retrogressive thaw slumps, observed at the Bykovsky Peninsula, Laptev Sea [36], and in

the Mackenzie Delta region – Beaufort Sea [37, 38], for example (Fig. 2a), as the sediment transport from ocean waves play a secondary role in coastal retreat in such formations. Erosion is also predominantly thermally driven in enclosed bays and in coastal segments protected by spits and barrier islands, where the fetch for ocean waves is limited [39], although barrier island themselves are often susceptible to wave abrasion [40]. In contrast, erosion of ice-rich cliffs, which occur extensively along the Beaufort and Laptev Sea coast for example [6–8], requires the mechanical action from ocean waves to open notches at the land-sea interface, causing the subsequent failure of often still frozen large blocks of permafrost. In some locations, the relative contribution of the thermal and mechanical drivers is more balanced than described above. At Muostakh Island in the Laptev Sea, for example, thermo-denudation and abrasion are estimated to contribute similarly to maintain erosion rates of up to 25 m/year [8]. In our erosion model, we initially assume equal contributions from the thermal and mechanical drivers at the pan-Arctic scale during the observational period. This assumes that deviations occur comparably in both directions. We also make extreme 10-90% and 90-10% scenarios of relative thermal-mechanical contributions to test the sensitivity of our results to that assumption (see Methods and Table S1). Attributing 90% of mechanical contribution yields about 15-20%s larger Arctic-mean coastal erosion projections by 2100 (and vice-versa), because the Arctic-mean wave exposure increases more than the thawing temperature exposure along the coast, with respect to their historical values (Fig. S1a).

Spatial variability of erosion

The thermal and mechanical drivers of erosion explain about 36-47% of its observed spatial variability in multiple linear regression models. On one hand, wave exposure, combined with ground-ice content, best explains the spatial variability of erosion in most of the coastal segments ($r = 0.69 \pm 0.12$, mean $\pm 2\sigma$, Fig. 2b), where erosion is not extremely high ($\sim 90^{\text{th}}$ percentile, $<$2.5 m/year). The local wave exposure information indeed integrates several important sources of erosion variability. Not only does wave exposure promote cliff abrasion and subsequent sediment transport, but it is also proportional to open-water season (OWS) duration, which has been suggested to be the first-order driver of coastal erosion rate variability [2, 32]. In addition, sea-ice melt, and thus increasing OWS duration, responds to increasing surface air temperature, which also drives permafrost thaw and thus erosion by thermo-denudation. On the other hand, spatial differences among segments of extremely high long-term erosion rates are best characterized by thawing temperature exposure combined with ground-ice content ($r = 0.61 \pm 0.42$, Fig. 2c). This suggests that thermo-denudation plays a more important role in driving coastal erosion rates at extreme-erosion segments, than at non-extreme ones. Among both extreme and non-extreme erosion segments, ground ice adds explanatory power, as it increases the susceptibility of permafrost to thaw and hence erosion. Our results are in accordance with previous work, which reported weak spatial correlations between ground-ice content and erosion rates [33]. Strong temporal correlations between erosion and thawing temperature exposure have also been reported for Muostakh Island – Laptev Sea [8], where erosion rates are often in the range between 10 and 20 m/year [8, 41]. We further combine the temporal evolution of the Arctic-mean erosion with its spatial

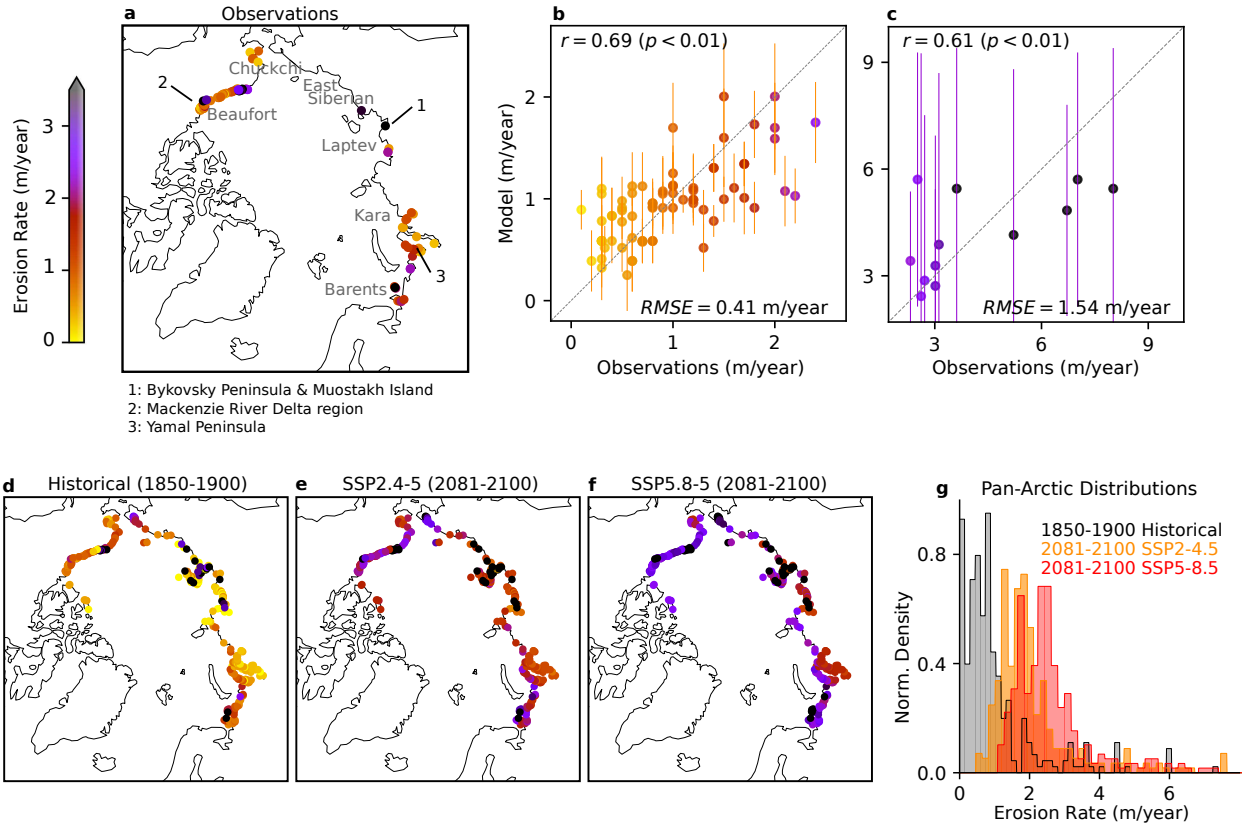

Figure 2: Observed and modelled erosion rate spatial variability. a) Observed long-term coastal erosion mean rates from the ACD database [33] used in this study (*see Methods*). Modelled against observed erosion rates in **(b)** non-extreme and **(c)** extreme erosion segments. Observed values are denoted by colored circles on the maps and on the scatter plots. Uncertainties represent 2σ confidence intervals from the distribution of regression coefficients. Modelled historical-mean (1850-1900) (**d**) and end-of-the-century (2081-2100) erosion rates according to the SSP2-4.5 (**e**) and SSP5-8.5 (**f**) scenarios. The histograms in **g** display the historical and projected erosion time-means from the maps in d, e and f. Distributions shift and spread over time.

distribution to make projections of erosion rates at the coastal segment resolution (Fig. 2d-f).

The geographical distribution of low and high-erosion segments does not change substantially from observations over time in our projections, which is partially a consequence of our model design, as explained by the three following reasons. First, we assume that the spatial model coefficients, empirically determined, remain unchanged throughout our simulations. Second, ground-ice content, an explanatory variable in our regression model, is also assumed constant over time. Third, our regression model accounts for only a fraction of the spatial variability in erosion, and may thus underestimate larger spatial changes to occur over time. Moreover, and independent from model design, local anomalies of the dynamical variables (i.e. local wave and thawing temperature exposure) are smaller in magnitude than their Arctic-mean increase. Therefore, our modelled changes in the spatial variability of erosion are small in comparison to its Arctic-mean increase. Nonetheless, our modelled spatial spread of erosion increases with time (Fig. 2g). The 5th-95th percentile range of erosion rate distributions increases from 3.6 (0-3.6) m/year in the historical period to 3.9 (0.9-4.8) and 4.2 (1.4-5.7) m/year in the SSP2-4.5 and SSP5-8.5 scenarios, respectively. Temporally resolved erosion rate observations are rare, often sparse in time, and only available at a relatively small number of locations [10]. Only with such observations, temporally resolved and

at the pan-Arctic scale, would empirical models be able to better constrain the temporal evolution of spatial variability of coastal erosion.

Spatial variability of organic carbon losses

The pan-Arctic OC loss from coastal erosion increases from 6.9 (1.5-12.3) TgC year^{-1} during the historical period to between 13.1 (6.4-19.7) TgC year^{-1} and 17.2 (9.0-25.4) TgC year^{-1} by the end of the century in the SSP2.4-5 and SSP5-8.5 scenarios, respectively (Fig. 3). For the present-day climate (i.e. the period for which erosion observations are available), we estimate a pan-Arctic OC loss from coastal erosion of 8.5 (3.3-13.7) TgC year^{-1}. Both our simulated present-climate mean and uncertainty range are comparable with previous estimates from observations [24, 33]. Our projections suggest a pan-Arctic OC flux increase by a factor of between 1.5 and 2.0 with respect to the present-day climate, or by a factor of between 1.9 and 2.5 by 2100 with respect to the historical period.

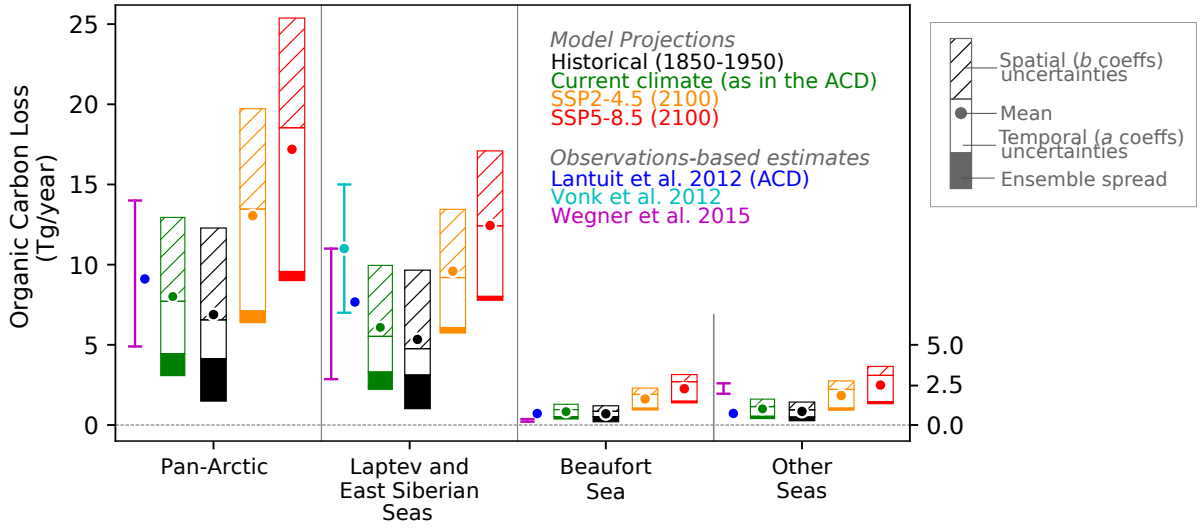

Figure 3: Projected organic carbon loss. Changes in organic carbon released annually by coastal erosion according to observations-based estimates and in our model simulations for the historical period (1850-1950), current climate (according to observations from the ACD [33]) and at the end of the 21st century (2081-2100) in the two future scenarios. The height of bars represent the total uncertainty of our projections, which we disentangle between ensemble spread, spatial and temporal erosion model components. Most of the uncertainties originate from the empirical estimates of the erosion model parameters (76-97%) and the smallest fraction to the ensemble spread (3-24%).

The Laptev and East Siberian Seas (LESS, Fig.2a) together account for about three quarters of the pan-Arctic OC losses in our simulations, in accordance with observations-based estimates [24]. This also holds truth for future scenarios. The reason for the relatively high OC fluxes from the LESS coast is twofold. First, the region comprises coastal segments of extremely rapid erosion, often between 10 and 20 m/year [8, 41]. Second, the LESS coast is dominated by Yedoma ice-complex deposits, where ground-ice concentration reaches more than 80% of soil volume [8, 42], and organic-carbon content is extremely high, reaching about 5% of weight [33]. From the LESS, we simulate a present-climate OC flux of 6.5 (2.4-10.6) TgC year^{-1}, comparable to the 2.9-11.0 TgC year^{-1} range estimated by Wegner et al. (2015) [24], and comprising the ACD

value of 7.7 TgC year^{-1} . In an extensive campaign over the LESS continental shelf, Vonk et al. (2012)[23] determined that about 20 TgC year^{-1} are buried in the LESS sediment, which would originate from a combination of coastal and seafloor erosion. Accounting for degradation before burial and assuming an equal contribution from coastal and subsea erosion, about 11 (7-15) TgC year^{-1} would be released by coastal erosion alone. The LESS estimate of Vonk et al. (2012) [23] is 43-57% larger than other observations-based estimates [24] and about 69% larger than our present-climate modelled value. These differences are likely due to extensive and high-resolution sampling, allowing for more accurate upscaling [23]. However, the uncertainties associated with the contribution between coastal and subsea erosion comprehend our modelled range (their Table S6 [23]). Therefore, an underestimation from our side is not conclusive. From the LESS coast, we project an increase in OC fluxes from 5.3 (1.0-9.6) TgC year^{-1} in the historical period to 9.6 (5.7-13.4) TgC year^{-1} in the SSP2-4.5 and 12.4 (7.8-17.1) TgC year^{-1} in the SSP5-8.5 scenarios by 2100, which translates to an increase by a factor of between 1.8 and 2.3.

The Beaufort Sea coast accounts for about half of the remaining fraction of pan-Arctic OC flux, releasing 0.9 (0.4-1.4) TgC year^{-1} during the present climate in our simulations, in agreement with the 0.7 TgC year^{-1} estimates from the ACD [33], however larger than previous estimates of 0.2-0.4 TgC year^{-1} [24] (Fig. 3). Hotspots of extreme erosion are also observed in the Beaufort Sea coast. Extensive field work has been recently carried out, especially in the Yukon coast region, showing increasing erosion rates and suggesting that the associated OC fluxes could have been previously underestimated [9, 22, 43–45]. We project an OC flux increase from the Beaufort Sea coast from 0.7 (0.2-1.2) TgC year^{-1} in the historical period to between 1.6 (0.9-2.3) TgC year^{-1} and 2.3 (1.4-3.1) TgC year^{-1} by 2100 in the SSP2-4.5 and SSP5-8.5 scenarios, respectively, translating to an increase by a factor of between 2.3 and 3.3. The remaining marginal Arctic Seas contribute with yearly OC fluxes at absolute amounts similar to those from Beaufort Sea in our projections, accounting for about 12-14% of the pan-Arctic totals.

Coastal erosion is estimated to sustain about one fifth of the total Arctic marine primary production at present-climate conditions [25]. Therefore, the projected additional OC loss could have a substantial impact on the Arctic marine biogeochemistry. However, the fate of the organic carbon released by Arctic coastal erosion is currently under active debate. Field work has shown that between about 13% and 65% of the OC released into the ocean by coastal erosion could settle in the marine sediment [44–46], slowing down remineralization. In the sediment, organic matter degradation would then take place at millennial time scales [47]. However, in the shallow nearshore zone, resuspension driven by waves and storm activity increases the residence time of OC in the water column, and allows for more effective remineralization [48]. Moreover, partial degradation of the eroded material takes place before it enters the ocean, releasing greenhouse gases directly to the atmosphere [22, 23, 49]. The OC degradation time scale thus also depends on its transit time onshore [49]. It is therefore challenging to determine short-term impacts from the projected additional OC fluxes from coastal erosion, as large uncertainties still remain regarding pathways of OC degradation.

We partition the uncertainty sources in our projections between three sources: ensemble spread,

temporal, and spatial erosion model components (see Methods). Our erosion model contributes the most to the uncertainties in our simulations: from about 76% of the total uncertainty range in the historical period and up to 97% by the end of the century in SSP5-8.5. The ensemble spread is responsible for the remaining 24% of the total uncertainty during the historical period, and for only 3% to 6% of the total range at the end of the future scenarios. The spatial component of the erosion model accounts for about half of the total range of uncertainties, on average, without significant changes in proportion over time. The fraction of uncertainties stemming from the temporal model component increases from about 33% of the total range in the historical period to about 55% by the end of the century in SSP5-8.5 due to the increasing magnitude of the erosion drivers. The distribution of sources of uncertainties in our projections is qualitatively similar between the pan-Arctic and the regional totals.

Sensitivity of erosion and carbon losses to climate change

The sensitivity of Arctic coastal erosion to climate change increases over time in our simulations, and is tightly related with the Arctic amplification (AA) [12] after its onset. Arctic coastal erosion increases more rapidly in response to increasing global mean surface air temperature (SAT) in the future scenarios than it does in the historical period. Before the mid 1970s, neither global nor Arctic-mean SAT decadal trends are consistently significantly positive yet (Fig. 4a). During this period, the correlation between the Arctic-mean erosion rate and the Arctic-mean SAT is weak ($r = 0.26 \pm 0.29$, mean $\pm 2\sigma$ range, Fig. 4b). However, after the 1970s, correlations between erosion and Arctic SAT increase substantially (SSP2-4.5: $r = 0.68 \pm 0.18$, SSP5-8.5: $r = 0.93 \pm 0.06$, 2081-2100 means), driven by the concurrent increasing trends. This turning point is also marked by the AA onset, when the Arctic SAT starts increasing at a faster pace than the global SAT, i.e. the AA factor is consistently larger than 1 (Fig. 4c). Therefore, the sensitivity of erosion to global SAT reflects the sensitivity of Arctic SAT to global SAT – quantified as the AA factor – after the AA onset, given the strong correspondence between erosion and the Arctic SAT at that time (Fig. 4d). The sharp increase of erosion sensitivity and the AA factor to their maximum values in the early 2000s is a signature from the so-called "hiatus" in global warming [50]. Global mean SAT stalls between the late 1990s and the early 2010s, while the erosion drivers continue to increase (Fig. S1b,c). Sensitivity values level off in the second half of the 21st Century, when global mean SAT trends decelerate. End-of-century sensitivities are lowest in the SSP2-4.5 scenario, when Arctic SAT trends decrease sharply to reach the also consistently decreasing global SAT trends, and the AA factor approaches one. In order to avoid the effect of the warming hiatus, we quantify erosion sensitivity considering the historical period until before the AA onset, and during the last 50 years in the scenario simulations.

The sensitivity of the Arctic-mean erosion rate to global mean SAT increases significantly from 0.18 ± 0.31 m year^{-1} °C^{-1} on average during the historical period until 1975, to at least double (between 0.40 ± 0.16 and 0.48 ± 0.21 m year^{-1} °C^{-1}) during the second half of the 21st Century following the SSP2-4.5 and SSP5-8.5 scenarios, respectively. This translates to an increase in the sensitivity of OC losses to climate warming from 1.4 TgC year^{-1} °C^{-1} in the historical period

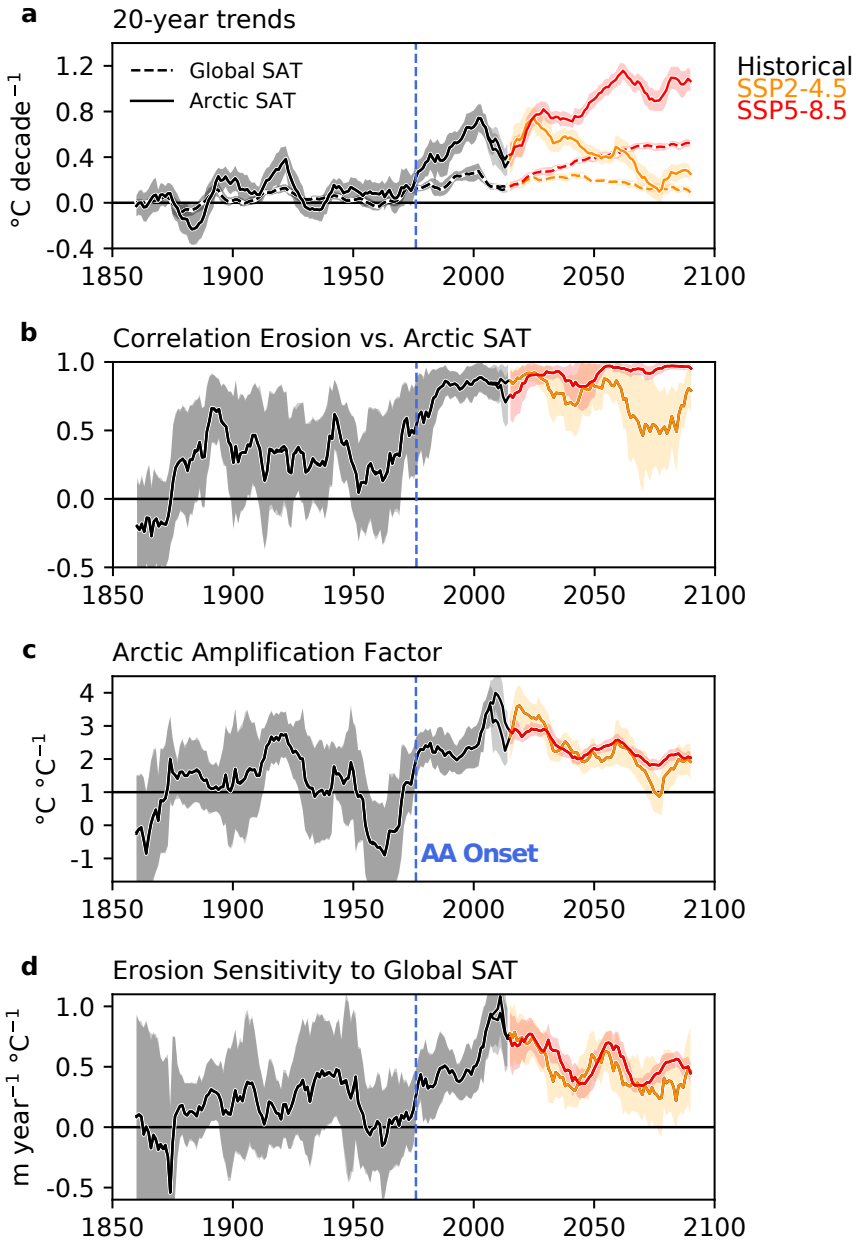

Figure 4: Sensitivity to climate change. **a**: 20-year running trends of global and Arctic mean surface air temperature (SAT). **b**: Correlations between Arctic-mean erosion rates and Arctic mean SAT. **c**: The Arctic Amplification (AA) factor, expressed as regression coefficients of Arctic SAT changes on global SAT. The AA onset is defined when the AA factor is larger than 1. **d**: Sensitivity of Arctic-mean erosion rates to climate, expressed regression coefficients on global SAT. Running-window lengths are 20 years in all plots. Different window lengths show qualitatively similar results (not shown). The AA onset (dashed blue line) takes place in 1976, when the Arctic SAT increases at a faster pace than the global mean SAT, i.e. the AA factor is larger then 1. After the the 1970s, the AA factor is consistently significantly larger than 1, except for late 21st-century in the SSP2-4.5 scenario, when global and Arctic mean SATs deaccelerated and 20-year trends are momentarily similar.

before until 1975, on average, to between 2.3 and 2.8 TgC year^{-1} °C^{-1} following the SSP2-4.5 and SSP5-8.5 scenarios, respectively.

The sensitivity parameters are useful tools to assess the state of Arctic coastal erosion increase and the associated OC fluxes at intermediate states or policy-based targets of global warming. It must be noted, however, that the sensitivity parameters usually assume linear relationships between the forcing and outcome variables [51]. Similarly, in our erosion model, we assume that the linear combination of thermal and mechanical drivers of erosion provides us with first-order large-scale information on the time evolution of Arctic coastal erosion, associated with a range of uncertainties and scenarios of proportionality factors. Non-linear effects could emerge, for example, from earlier onsets of the storm season overlapping with longer-lasting positive temperatures into fall. We do not consider sea-level change in our projections. Adding sea-level change as a temporal driver of erosion would increase future erosion and the sensitivity parameters, if it increases proportionally faster than our thermal and mechanical drivers with respect to the historical period. We do not directly consider episodic water level changes due to storms, which are relevant for coastal abrasion and sediment transport. However, by using a global dynamical wave model, and integrating yearly wave exposure at the coastal-segment level, we do incorporate the effect of storms in our mechanical driver of erosion. Our erosion model, relatively simple in comparison with higher-resolution and process-based strategies [52–57], does not intended to represent all processes, often of fine spatial scale (order of meters or less), associated with the erosion of the Arctic coast. Here, we empirically parameterize the role of the the main, first-order drivers of Arctic coastal erosion at larger-scales, compatible with the resolution and mechanisms represented in ESMs (order of tens or hundreds of kilometers). Future work on coastal erosion modelling is necessary to constrain our relatively large uncertainties. Nonetheless, our semi-empirical approach allows us to make pan-Arctic projections of coastal erosion, its associated OC fluxes, and thus estimate the magnitude, timing and sensitivity of their increase to global warming.

Conclusions

We present a semi-empirical model for coastal erosion to make 21st-century pan-Arctic projections of erosion rates and associated organic carbon (OC) losses. Our model accounts for temporal and spatial variability of erosion, combining wave and thawing temperature exposure with ground-ice content as explanatory variables. With our approach, we are able to provide estimates of magnitude, timing and sensitivity of Arctic coastal erosion increase to climate change. The Arctic-mean erosion rate increases by a factor of between 2.2 and 2.9 from the historical period (1850-1900) to the end of the 21st Century following the SSP2-4.5 and the SSP5-8.5 scenarios, respectively. The associated pan-Arctic OC flux increases by a factor of 1.9-2.5 at the same time, reaching up to 17.2 (9.0-25.4, two standard-deviation range) TgC year^{-1} in the SSP5-8.5 scenario. Our projections show that Arctic coastal erosion is very likely (at least 90% probability) to exceed its historical range of variability before end of the century, even in the intermediate-emission scenario. We estimate that the sensitivity of Arctic coastal erosion to climate also increases with time, following the Arctic amplification after its onset in the 1970s, due to the strong relationship between

erosion and Arctic SAT at that time. During the second half of the century, one degree of global warming is associated with an increase of the Arctic-mean erosion by about 0.4-0.5 m/year and 2.3-2.8 TgC/year of associated OC carbon loss, equivalent to about 5-8% of the present-climate OC yearly flux from the Arctic rivers into the Ocean. Arctic coastal erosion will increase more rapidly in the future in response climate change, roughly doubling in rates by 2100, and likely reaching values unseen before in the past century. Our projections allow future work to investigate the impact of Arctic coastal erosion on the permafrost-climate feedback, and the future evolution of the Arctic Ocean's ecosystems and its role as a global carbon sink. Moreover, our results should also inform policy makers on coastal conservation and socioeconomic planning at the pan-Arctic level, focusing on the sustainable future of Arctic coastal communities.

Acknowledgements

D.M.N., M.D., P.O., T.I. and V.B. are funded by European Union's Horizon 2020 research and innovation programme under grant agreement number 773421 - project "Nunataryuk". D.M.N., P.P., A.B. T.I., J.B. and V.B. are funded by the Deutsche Forschungsgemeinschaft (DFG, German Research Foundation) under Germany's Excellence Strategy – EXC 2037 'CLICCS - Climate, Climatic Change, and Society' – Project Number: 390683824, contribution to the Center for Earth System Research and Sustainability (CEN) of Universität Hamburg.

Competing Interests

The authors declare no competing interests.

Authors' contributions

D.M.N, M.D., J.B. and V.B. conceived and designed the study. D.M.N., P.P., M.D., J.B. and V.B. designed the erosion model. D.M.N. and M.D. performed the Ocean wave simulations. All authors analyzed and discussed the results. All authors wrote and reviewed the paper.

Methods

Data

Arctic coastal observations.

We use the Arctic Coastal Dynamics (ACD) database [33] as our observational reference. The ACD compiles several sources of data and provides a list of variables for a total of 1314 coastal segments along the Arctic coast, including: long-term erosion mean rates, organic carbon concentration, soil bulk density, ground-ice fraction, mean elevation and length. From the 1314 segments, we take those classified as erosive and non-lithified, which excludes segments from the rocky coasts in Greenland and in the Canadian Archipelago and other segments that present stable or

aggrading dynamics. We also select segments containing excess ice, which excludes all the non-erosive segments from Svalbard, for example. We this work with a subset of 306 coastal segments in our analysis.

Reanalysis

We take 2-meter air temperature and significant wave heights from ERA20C reanalysis [58] as empirical variables in our coastal erosion model. Data are taken in the same periods for which the erosion rates are provided in the ACD. The temperature and wave data have $\sim 1.12^o$ (atmosphere) and 1.5^o (waves) horizontal resolution. We assign the closest land grid cell in ERA20C from its atmospheric grid to ACD segments, and two rows of adjacent cells from the ocean grid.

Climate projections

To force our coastal erosion model, we use a 10-member ensemble of simulations from the Max Planck Institute Earth System Model (MPI-ESM) version 1.2 in its low-resolution configuration [59] performed for the Coupled Model Intercomparison Project phase 6 (CMIP6) [34]. In this configuration, the atmospheric component ECHAM6.3 has horizontal resolution of T63 ($\sim$200 km), and 47 vertical levels. The oceanic component MPIOM1.6 uses the curvilinear grid GR1.5, which has mean horizontal resolution of $\sim$150 km and 40 vertical levels. We use the historical simulations (1850-2014) and two future Shared Socioeconomic Pathway (SSP) scenarios for the 21st century projections (2015-2100), namely: the SSP2-4.5 and the SSP5-8.5, which represent a mid-range and a high-end emission scenario, respectively. This range of scenarios is realistic it terms of current cumulative CO_2 emissions [35].

Ocean wave simulations

We use the wave model WAM [60] to generate a 10-member ensemble of global waves for historical, SSP2-4.5 and SSP5-8.5 scenarios, forced by the MPI-ESM ensemble. In our setup, WAM has 1$^{\text{o}}$ grid resolution and is forced with daily sea-ice concentration (threshold of 15% to define open-water), 6-hourly 10-meter winds, and a realistic ETOPO2-based bathymetry as boundary conditions.

Semi-empirical Arctic coastal erosion model

We present a simplified model for Arctic coastal erosion, compatible with the scales of Earth system models. Our model considers the dominant physical thermal and mechanical drivers of erosion, also referred to as thermal-abrasion (TA) and thermal-denudation (TD) [1]. The model is constrained to only simulate erosion at the presence of ground ice and at the absence of coastal sea ice. We use an empirical approach to quantify the relationship between the physical drivers, constraints and the erosion rates, by comparing the observations from the ACD with ERA20C reanalysis. The empirically estimated parameters are then applied to all coastal segments, which provides us with erosion rates in the pan-Arctic scale. Our model has yearly time resolution, and the spatial resolution follows the definitions of the ACD coastal segments.

The total erosion E(t,x) [m year^{-1}], defined in every year t and coastal segment $x(lat, lon)$, is given as a combination of a temporal and a spatial component.

$$E(x,t) = \overline{E}(t) + \Delta E(x,t) \tag{1}$$

The temporal component represents the temporal evolution of the Arctic-mean erosion $\overline{E}(t)$ [m year^{-1}]. The spatial component $\Delta E(x,t)$ [m year^{-1}] represents local departures from the Arctic mean at every year and coastal segment, providing spatially distributed values of erosion. Hereafter, we use "Arctic mean", denoted by the overline, to refer to means along the Arctic coast. All data associated with ACD coastal segments are weighted by segment lengths in the computation of means.

The temporal component

The temporal component of our model is a linear combination of Arctic means of the thermal and mechanical drivers of erosion.

$$\overline{E}(t) = a_{TD}\,\overline{T}(t) + \, a_{TA}\,\overline{H}(t) \tag{2}$$

The thermal driver of erosion is represented by Arctic-mean yearly-accumulated daily-mean positive 2-meter air temperatures $\overline{T}$(t) [°C day year^{-1}], also commonly known as positive degree-days or thawing-degree days. The mechanical driver of erosion is represented by Arctic-mean yearly-accumulated daily significant wave heights $\overline{H}$(t) [m day year^{-1}].

We empirically estimate the linear coefficients a_{TA} [m m^{-1} day^{-1} year] and a_{TD} [^{o}C m^{-1} day^{-1} year] by scaling the Arctic-mean physical drivers, from ERA20C reanalysis, with the observed coastal erosion rates from the ACD. This is done for the reference time t_{obs}, during which observations are available.

$$a_{TA} = q\frac{\overline{E}_{obs}}{\overline{H}(t_{obs})} \tag{3}$$

$$a_{TD} = (1-q)\frac{\overline{E}_{obs}}{\overline{T}(t_{obs})} \tag{4}$$

We assume that the thermal and mechanical drivers $a_{TD}\overline{T}(t)$ and $a_{TA}\overline{H}(t)$ contribute in equal proportions to the Arctic-mean erosion during the reference time. We do that by setting the proportionality factor q to 0.5. We test the sensitivity of our results to this assumption by making scenarios with $q = 0.1$ and $q = 0.9$ (see Table S1 and Fig. S1a in the supplementary material).

The spatial component

The spatial component of our erosion model calculates local erosion anomalies with respect to the Arctic-mean temporal evolution, and consists of two multiple linear regression (MLR) models.

We split the coastal segments in two groups by classifying them between *extreme* and *non-extreme* with respect to erosion, using 2.5 m/year as a threshold ($\sim$90*th* percentile). We do not find a distinct separation between extreme and non-extreme segments in terms of geographical location (Fig. 2a), neither in terms of coastal morphology. Both groups show similar distributions of ground-ice content, mean cliff height, bathymetric profile, bulk density, as well as mean thermal and mechanical forcings derived from thawing temperature and ocean waves, for example (not shown). We test a comprehensive number of combinations of dynamical and geomorphological parameters as explanatory variables in MLR models, simultaneously maximizing goodness-of-fit and penalizing model complexity (Table S3). We fit MLR models using the usual Ordinary Least Square (OLS) method. The goodness-of-fit of models is assessed with the proportion of explained variance and root-mean squared error (RMSE). Since increasing the number of combined explanatory variables necessarily increases the model fit and may lead to overfitting, we penalize model complexity by assessing the changes in the Akaike Information Criterion (ΔAIC) in parallel. The best performing combination of covariates is the one which maximizes correlation (or proportion of explained variance) and minimizes RMSE and ΔAIC (Fig. S2). We train the spatial component of our erosion model only on those segments classified as "high quality" with respect to erosion data. We include medium-quality segments to train the model for the high-erosion case to increase our sample size and thus also statistical robustness. We validate each combination of regression coefficients with unseen data by performing a leave-one-out cross validation test. We use a Bootstrap approach with 10 thousand sampling iterations to obtain distributions of model coefficient estimates, and thus their associated uncertainties.

Three variables compose the best performing combinations: a) daily-mean thawing temperature exposure, expressed as the yearly-accumulated daily positive temperature divided by the number of positive-temperature days per year T_{day} [°C year^{-1}], b) daily-mean wave exposure, expressed as the yearly-accumulated daily significant wave heights divided by the number of open-water days per year H_{day} [m year^{-1}], and c) ground-ice content θ [% of soil volume]. On one hand, combining ground-ice content with daily-mean wave exposure (θ+H_{day}) explains about 47% of the observed spatial variance among non-extreme (2.5 m/year threshold) erosion segments ($r = 0.69$, 9-95$^{\text{th}}$-percentile range: $r = 0.60 - 0.78$, Fig. 2b, Fig. S3a). On the other hand, combining ground-ice content with the daily-mean thawing temperature exposure (θ+T_{day}) explains about 36% of the variance among extreme-erosion segments ($r = 0.61$, 9-95$^{\text{th}}$-percentile range: $r = 0.31 - 0.94$, Fig. 2c, Fig. S3a). The linear regression coefficients b obtained with the selected variable combinations are statistically significant ($p < 0.01$).

$$\Delta E(x,t) = \begin{cases} b_\theta \Delta\theta(x) + b_H \Delta H_{day}(x,t) & \text{if } E_{obs}(x) < 2.5 \text{ m year}^{-1} \\ b'_\theta \Delta\theta(x) + b_T \Delta T_{day}(x,t) & \text{otherwise} \end{cases} \tag{5}$$

Swapping the combinations and groups, that is, using θ+H_{day} for the extreme and θ+T_{day} for the non-extreme erosion segments, yields overall poorer fits (Fig. S3a,b) and less robust estimation of regression coefficients (Fig. S3c-e). We also test the sensitivity of these results to the choice

of the threshold to define extreme erosion. Allowing for an overlap between the extreme and non-extreme segments by lowering the threshold to 2.0 m/year, for example, increases the robustness of the T_{day} regression coefficient estimate for the extreme group (Fig. S3d) by increasing the number of data points, and yields a similar fit to that of the higher threshold (θ+T_{day} in Fig. S3a,b) and also similar ground-ice coefficients (θ+T_{day} in Fig. 3Sc).

Finally, the total erosion is constrained to the open-water period, and set to zero whenever and wherever sea-ice concentration (SIC) is above 15% at the coast. Combining the temporal (Eq. 2) and spatial (Eq. 5) components into our total erosion model (Eq. 1), conditioned by open-water and the extreme-erosion threshold, our model assumes the complete form:

$$E(x,t) = \begin{cases} a_{TD}\,\overline{T}(t) + a_{TA}\,\overline{H}(t) + \begin{cases} b_\theta \Delta\theta(x) + b_H \Delta H_{day}(x,t) & \text{if } E_{obs}(x) < 2.5 \text{ m/year} \\ b'_\theta \Delta\theta(x) + b_T \Delta T_{day}(x,t) & \text{if } E_{obs}(x) \geq 2.5 \end{cases} & \text{if } \mathit{SIC}\,(x) < 15\% \\ 0 & \text{if } \mathit{SIC}\,(x) \geq 15\% \end{cases} \tag{6}$$

Bias correction

Before forcing the erosion model with MPI-ESM data, we adjust the historical and scenario simulatins for climate biases. The bias is removed between ERA20C data (used to estimate our model parameters) and MPI-ESM ensemble means at the coastal segments and reference periods from observations. The modelled distributions are shifted and scaled, so that their means and spread fit those of ERA20C at the reference time.

Organic carbon fluxes

We translate linear erosion rates into volumetric erosion rates E_{vol} [m^3 $year^{-1}$], sediment fluxes S [Kg $year^{-1}$], and carbon fluxes C_{flux} [Kg $year^{-1}$], considering the mean geometry and ground properties of each coastal segment.

$$\begin{aligned} E_{vol}(x,t) &= E(x,t)\; L(x)\; h(x) \\ S(x,t) &= E_{vol}(x,t)\; (1-\theta(x))\; \rho(x) \\ C_{flux}(x,t) &= S(x,t)\; C_{conc.}(x) \end{aligned} \tag{7}$$

where L and h are the segments' mean length and elevation [m], θ is the ground-ice content [% volume], ρ is the soil bulk density [Kg/m^3], and $C_{conc.}$ is the organic carbon concentration [% weight]. We integrate over the coastal segments:

$$\overline{C}_{flux}(t) = \sum_x C_{flux}(x,t) \tag{8}$$

to obtain the total Arctic flux.

Sensitivity to climate change

We estimate the sensitivity of the organic carbon release by Arctic coastal erosion to climate change following the approach of Friedlingstein et al. (2006) [51]; however, with a simplified set of tools. In their work, Friedlingstein et al. compare pairs of "coupled" and "uncoupled" simulations, where the increasing atmospheric CO_2 concentration either affects climate, or is neutral in terms of radiative effect. This pairwise comparison is necessary because the land-atmosphere and ocean-atmosphere carbon fluxes respond to changes in both climate and atmospheric CO_2 concentrations. Therefore, the difference between their coupled and uncoupled simulations provide the isolated effect of the CO_2-induced changes in climate on carbon fluxes from the effect of the changing atmospheric CO_2 concentration. In our case, changes in atmospheric CO_2 alone do not induce any Arctic coastal erosion response, if not by its radiative effect. An uncoupled simulation, where CO_2 does not induce a change in climate, would not yield any change in the organic carbon released by Arctic coastal erosion. Therefore, we can estimate the sensitivity of the organic carbon release by Arctic coastal erosion to climate γ [TgC year^{-1} ^{o}C^{-1}] by comparing changes in global mean surface temperature and the resulting changes in carbon fluxes from erosion.

Probability and onset of emergence from the historical range

We define the yearly probability density distribution of a modelled variable ψ as the normal distribution $N(t)$ at year t. The mean of $N(t)$ is the ensemble mean and its standard deviation is the ensemble standard deviation (plus the standard deviation of the distribution of erosion model uncertainties in specific situations, made clear in the text). Similarly, the historical range of a modelled variable ψ is the normal distribution fitted to its average over the period 1850-1950 N_{hist}. We calculate the area of distributions $A_{hist} = \int N_{hist} d\psi$ and $A(t) = \int N(t) d\psi$ to determine their overlap $A_{hist} \cap A(t)$. We define the probability of emergence from the historical range $P(t)$, i.e. the probability that $N(t)$ be different from N_{hist}, as the fraction of $A(t)$ that emerges from A_{hist}:

$$P(t) = \frac{A(t) - A_{hist} \cap A(t)}{A(t)} \times 100 \ [\%] \tag{9}$$

We define the onset of emergence as the year when the ensemble mean is larger than $\mu + 2\sigma$ from historical range N_{hist}.

Estimation of uncertainties

All ranges of uncertainties, except when clearly stated otherwise, are calculated with a Bootstrap method, which suits cases where the number of data is relatively small. From any vector $\mathbf{X}$ of arbitrary length, a large number (i.e. 10 thousand) of vectors $\mathbf{X}^i$ ($i = 1,\ 2,\ \cdots\ 10\text{k}$) is generated by sampling with replacement from $\mathbf{X}$. The uncertainty of any statistics of $\mathbf{X}$ is estimated from the distribution of i realizations of the statistics obtained from $\mathbf{X}^i$.

References

[1] Aré, F. E. "Thermal abrasion of sea coasts (part I)". In: *Polar Geography and Geology* 12.1 (1988), pp. 1–1. DOI: 10.1080/10889378809377343.

[2] Overeem, Irina et al. "Sea ice loss enhances wave action at the Arctic coast". In: *Geophysical Research Letters* 38.17 (2011). DOI: https://doi.org/10.1029/2011GL048681.

[3] Casas-Prat, Mercè and Wang, Xiaolan L. "Sea Ice Retreat Contributes to Projected Increases in Extreme Arctic Ocean Surface Waves". In: *Geophysical Research Letters* 47.15 (2020), e2020GL088100. DOI: https://doi.org/10.1029/2020GL088100.

[4] Barnhart, K. R., Overeem, I., and Anderson, R. S. "The effect of changing sea ice on the physical vulnerability of Arctic coasts". In: *Cryosphere* 8.5 (2014), pp. 1777–1799. DOI: 10.5194/tc-8-1777-2014.

[5] Barnhart, Katherine R. et al. "Mapping the future expansion of Arctic open water". In: *Nature Climate Change* 6.3 (2016), pp. 280–285. DOI: 10.1038/nclimate2848.

[6] Jones, B M et al. "Increase in the rate and uniformity of coastline erosion in Arctic Alaska". In: *Geophysical Research Letters* 36.3 (2009). DOI: 10.1029/2008GL036205.

[7] Jones, Benjamin M et al. "A decade of remotely sensed observations highlight complex processes linked to coastal permafrost bluff erosion in the Arctic". In: *Environmental Research Letters* 13.11 (2018), p. 115001. DOI: 10.1088/1748-9326/aae471.

[8] Günther, F et al. "Observing Muostakh disappear: Permafrost thaw subsidence and erosion of a ground-ice-rich Island in response to arctic summer warming and sea ice reduction". In: *Cryosphere* 9.1 (2015), pp. 151–178. DOI: 10.5194/tc-9-151-2015.

[9] Irrgang, Anna M. et al. "Variability in Rates of Coastal Change Along the Yukon Coast, 1951 to 2015". In: *Journal of Geophysical Research: Earth Surface* 123.4 (2018), pp. 779–800. DOI: https://doi.org/10.1002/2017JF004326.

[10] Jones B. M. Irrgang A. M., Farquharson A. M. et al. "Coastal Permafrost Erosion". In: *Arctic Report Card 2020*. Ed. by Frey K. E. et al. 2020. DOI: https://doi.org/10.25923/e47w-dw52.

[11] Stroeve, Julienne and Notz, Dirk. "Changing state of Arctic sea ice across all seasons". In: *Environmental Research Letters* 13.10 (2018), p. 103001. DOI: 10.1088/1748-9326/aade56.

[12] Serreze, MC et al. "The emergence of surface-based Arctic amplification". In: *The Cryosphere* 3.1 (2009), p. 11. DOI: https://doi.org/10.5194/tc-3-11-2009.

[13] Cohen, J et al. "Recent Arctic amplification and extreme mid-latitude weather". In: *Nature Geoscience* 7.9 (2014), pp. 627–637. DOI: 10.1038/ngeo2234.

[14] Biskaborn, Boris K. et al. "Permafrost is warming at a global scale". In: *Nature Communications* 10.1 (Dec. 2019), p. 264. DOI: 10.1038/s41467-018-08240-4.

[15] Landrum, Laura and Holland, Marika M. "Extremes become routine in an emerging new Arctic". In: *Nature Climate Change* (2020), pp. 1–8. DOI: https://doi.org/10.1038/s41558-020-0892-z.

[16] Notz, Dirk and Community, SIMIP. "Arctic Sea Ice in CMIP6". In: *Geophysical Research Letters* 47.10 (2020), e2019GL086749. DOI: https://doi.org/10.1029/2019GL086749.

[17] Dobrynin, M., Murawsky, J., and Yang, S. “Evolution of the global wind wave climate in CMIP5 experiments”. In: *Geophysical Research Letters* 39.17 (Sept. 2012). DOI: 10.1029/2012GL052843.

[18] Dobrynin, Mikhail et al. “Detection and attribution of climate change signal in ocean wind waves”. In: *Journal of Climate* 28.4 (2015), pp. 1578–1591. DOI: 10.1175/JCLI-D-13-00664.1.

[19] Casas-Prat, Mercè and Wang, Xiaolan L. “Projections of Extreme Ocean Waves in the Arctic and Potential Implications for Coastal Inundation and Erosion”. In: *Journal of Geophysical Research: Oceans* 125.8 (2020), e2019JC015745. DOI: https://doi.org/10.1029/2019JC015745.

[20] Schaefer, Kevin et al. “The impact of the permafrost carbon feedback on global climate”. In: *Environmental Research Letters* 9.8 (2014), p. 085003. DOI: 10.1088/1748-9326/9/8/085003.

[21] Schuur, Edward AG et al. “Climate change and the permafrost carbon feedback”. In: *Nature* 520.7546 (2015), pp. 171–179. DOI: https://doi.org/10.1038/nature14338.

[22] Tanski, George et al. “Rapid CO 2 release from eroding permafrost in seawater”. In: *Geophysical Research Letters* 46 (2019), pp. 11244–11252. DOI: 10.1029/2019GL084303.

[23] Vonk, Jorien E et al. “Activation of old carbon by erosion of coastal and subsea permafrost in Arctic Siberia”. In: *Nature* 489.7414 (2012), pp. 137–140. DOI: https://doi.org/10.1038/nature11392.

[24] Wegner, Carolyn et al. “Variability in transport of terrigenous material on the shelves and the deep Arctic Ocean during the Holocene”. In: *Polar Research* 34.1 (2015). DOI: 10.3402/polar.v34.24964.

[25] Terhaar, Jens et al. “Around one third of current Arctic Ocean primary production sustained by rivers and coastal erosion”. In: *Nature Communications* 12.169 (2021). DOI: https://doi.org/10.1038/s41467-020-20470-z.

[26] Koven, Charles D, Riley, William J, and Stern, Alex. “Analysis of permafrost thermal dynamics and response to climate change in the CMIP5 Earth System Models”. In: *Journal of Climate* 26.6 (2013), pp. 1877–1900. DOI: https://doi.org/10.1175/JCLI-D-12-00228.1.

[27] Burke, E. J., Zhang, Y., and Krinner, G. “Evaluating permafrost physics in the Coupled Model Intercomparison Project 6 (CMIP6) models and their sensitivity to climate change”. In: *The Cryosphere* 14.9 (2020), pp. 3155–3174. DOI: 10.5194/tc-14-3155-2020.

[28] Turetsky, Merritt R et al. “Carbon release through abrupt permafrost thaw”. In: *Nature Geoscience* 13.2 (2020), pp. 138–143. DOI: https://doi.org/10.1038/s41561-019-0526-0.

[29] Pihl, Erik et al. “10 New Insights in Climate Science 2020 - a Horizon Scan”. In: *Global Sustainability* 4 (2021), pp. 1–65. DOI: 10.1017/sus.2021.2.

[30] Fritz, Michael, Vonk, Jorien E., and Lantuit, Hugues. “Collapsing Arctic coastlines”. In: *Nature Climate Change* 7.1 (2017), pp. 6–7. DOI: 10.1038/nclimate3188.

[31] Turetsky, Merritt R et al. *Permafrost collapse is accelerating carbon release*. 2019. DOI: https://doi.org/10.1038/d41586-019-01313-4.

[32] Nielsen, David Marcolino et al. “Coastal Erosion Variability at the Southern Laptev Sea Linked to Winter Sea Ice and the Arctic Oscillation”. In: *Geophysical Research Letters* 47.5 (2020), e2019GL086876. DOI: 10.1029/2019GL086876.

[33] Lantuit, Hugues et al. “The Arctic Coastal Dynamics Database: A New Classification Scheme and Statistics on Arctic Permafrost Coastlines”. In: *Estuaries and Coasts* 35.2 (2012), pp. 383–400. DOI: 10.1007/s12237-010-9362-6.

[34] O’Neill, B. C. et al. “The Scenario Model Intercomparison Project (ScenarioMIP) for CMIP6”. In: *Geoscientific Model Development* 9.9 (2016), pp. 3461–3482. DOI: 10.5194/gmd-9-3461-2016.

[35] Schwalm, Christopher R., Glendon, Spencer, and Duffy, Philip B. “RCP8.5 tracks cumulative CO_2 emissions”. In: *Proceedings of the National Academy of Sciences* 117.33 (2020), pp. 19656–19657. DOI: 10.1073/pnas.2007117117.

[36] Lantuit, Hugues et al. “Coastal erosion dynamics on the permafrost-dominated Bykovsky Peninsula, north Siberia, 1951-2006”. In: *Polar Research* 30.SUPPL.1 (2011). DOI: 10.3402/polar.v30i0.7341.

[37] Lantz, Trevor C. and Kokelj, Steven V. “Increasing rates of retrogressive thaw slump activity in the Mackenzie Delta region, N.W.T., Canada”. In: *Geophysical Research Letters* 35.6 (2008). DOI: https://doi.org/10.1029/2007GL032433.

[38] Lantuit, H. and Pollard, W.H. “Fifty years of coastal erosion and retrogressive thaw slump activity on Herschel Island, southern Beaufort Sea, Yukon Territory, Canada”. In: *Geomorphology* 95.1 (2008), pp. 84–102. DOI: https://doi.org/10.1016/j.geomorph.2006.07.040.

[39] Baranskaya, Alisa et al. “The Role of Thermal Denudation in Erosion of Ice-Rich Permafrost Coasts in an Enclosed Bay (Gulf of Kruzenstern, Western Yamal, Russia)”. In: *Frontiers in Earth Science* 8 (2021), p. 659. DOI: 10.3389/feart.2020.566227.

[40] Farquharson, Louise M et al. “Temporal and spatial variability in coastline response to declining sea-ice in northwest Alaska”. In: *Marine Geology* 404 (2018), pp. 71–83. DOI: https://doi.org/10.1016/j.margeo.2018.07.007.

[41] Grigoriev, MN. “Coastal retreat rates at the Laptev Sea key monitoring sites”. In: *PANGAEA* (2019). DOI: https://doi.org/10.1594/PANGAEA.905519.

[42] Fuchs, M. et al. “Carbon and nitrogen pools in thermokarst-affected permafrost landscapes in Arctic Siberia”. In: *Biogeosciences* 15.3 (2018), pp. 953–971. DOI: 10.5194/bg-15-953-2018.

[43] Ramage, Justine L. et al. “Terrain controls on the occurrence of coastal retrogressive thaw slumps along the Yukon Coast, Canada”. In: *Journal of Geophysical Research: Earth Surface* 122.9 (2017), pp. 1619–1634. DOI: https://doi.org/10.1002/2017JF004231.

[44] Couture, Nicole J. et al. “Coastal Erosion of Permafrost Soils Along the Yukon Coastal Plain and Fluxes of Organic Carbon to the Canadian Beaufort Sea”. In: *Journal of Geophysical Research: Biogeosciences* 123.2 (2018), pp. 406–422. DOI: https://doi.org/10.1002/2017JG004166.

[45] Grotheer, H. et al. “Burial and Origin of Permafrost-Derived Carbon in the Nearshore Zone of the Southern Canadian Beaufort Sea”. In: *Geophysical Research Letters* 47.3 (2020), e2019GL085897.

[46] Hilton, Robert G et al. “Erosion of organic carbon in the Arctic as a geological carbon dioxide sink”. In: *Nature* 524.7563 (2015), pp. 84–87. DOI: https://doi.org/10.1038/nature14653.

[47] Bröder, Lisa et al. “Bounding cross-shelf transport time and degradation in Siberian-Arctic land-ocean carbon transfer”. In: *Nature communications* 9.1 (2018), pp. 1–8. DOI: https://doi.org/10.1038/s41467-018-03192-1.

[48] Jong, Dirk et al. “Nearshore Zone Dynamics Determine Pathway of Organic Carbon From Eroding Permafrost Coasts”. In: *Geophysical Research Letters* 47.15 (2020), e2020GL088561. DOI: https://doi.org/10.1029/2020GL088561.

[49] Tanski, George et al. “Permafrost Carbon and CO2 Pathways Differ at Contrasting Coastal Erosion Sites in the Canadian Arctic”. In: *Frontiers in Earth Science* 9 (2021), p. 207. DOI: 10.3389/feart.2021.630493.

[50] Kosaka, Yu and Xie, Shang-Ping. “Recent global-warming hiatus tied to equatorial Pacific surface cooling”. In: *Nature* 501.7467 (2013), pp. 403–407. DOI: https://doi.org/10.1038/nature12534.

[51] Friedlingstein, Pierre et al. “Climate–carbon cycle feedback analysis: results from the C4MIP model intercomparison”. In: *Journal of climate* 19.14 (2006), pp. 3337–3353. DOI: https://doi.org/10.1175/JCLI3800.1.

[52] Hoque, Md. Azharul and Pollard, Wayne H. “Arctic coastal retreat through block failure”. In: *Canadian Geotechnical Journal* 46.10 (2009), pp. 1103–1115. DOI: https://doi.org/10.1139/T09-058.

[53] Ravens, Thomas M. et al. “Process-Based Coastal Erosion Modeling for Drew Point, North Slope, Alaska”. In: *Journal of Waterway, Port, Coastal, and Ocean Engineering* 138.2 (2011), pp. 122–130. DOI: 10.1061/(asce)ww.1943-5460.0000106.

[54] Barnhart, Katherine R. et al. “Modeling erosion of ice-rich permafrost bluffs along the Alaskan Beaufort Sea coast”. In: *Journal of Geophysical Research: Earth Surface* 119.5 (2014), pp. 1155–1179. DOI: 10.1002/2013JF002845.

[55] Thomas, Matthew A. et al. “Geometric and Material Variability Influences Stress States Relevant to Coastal Permafrost Bluff Failure”. In: *Frontiers in Earth Science* 8 (2020), p. 143. DOI: 10.3389/feart.2020.00143.

[56] Frederick, Jennifer et al. “A thermo-mechanical terrestrial model of Arctic coastal erosion”. In: *Journal of Computational and Applied Mathematics* (2021), p. 113533. DOI: https://doi.org/10.1016/j.cam.2021.113533.

[57] Rolph, R. et al. “ArcticBeach v1.0: A physics-based parameterization of pan-Arctic coastline erosion”. In: *Geoscientific Model Development Discussions* 2021 (2021), pp. 1–26. DOI: 10.5194/gmd-2021-28.

[58] Poli, Paul et al. “ERA-20C: An atmospheric reanalysis of the twentieth century”. In: *Journal of Climate* 29.11 (2016), pp. 4083–4097. DOI: 10.1175/JCLI-D-15-0556.1.

[59] Mauritsen, Thorsten et al. “Developments in the MPI-M Earth System Model version 1.2 (MPI-ESM1.2) and Its Response to Increasing CO2”. In: *Journal of Advances in Modeling Earth Systems* 11.4 (2019), pp. 998–1038. DOI: https://doi.org/10.1029/2018MS001400.

[60] The WAMDI Group. “The WAM Model—A Third Generation Ocean Wave Prediction Model”. In: *Journal of Physical Oceanography* 18.12 (1988), pp. 1775–1810.

Supplementary Files

This is a list of supplementary files associated with this preprint. Click to download.

- CoastalErosionSuplement20210608.pdf